Cell

Structures of *Drosophila* Cryptochrome and Mouse Cryptochrome1 Provide Insight into Circadian Function

Anna Czarna,[1,2,5] Alex Berndt,[3,6] Hari Raj Singh,[1] Astrid Grudziecki,[4] Andreas G. Ladurner,[1] Gyula Timinszky,[1] Achim Kramer,[4] and Eva Wolf[1,*]

[1]Department of Physiological Chemistry and Centre for Integrated Protein Science Munich (CIPSM), Butenandt Institute, Ludwig Maximilians University of Munich, Butenandtstrasse 5, 81377 Munich, Germany

[2]Department of Structural Cell Biology, Max Planck Institute of Biochemistry, Am Klopferspitz 18, 82152 Martinsried, Germany

[3]Max Planck Institute of Molecular Physiology, Otto-Hahn-Strasse 11, 44227 Dortmund, Germany

[4]Laboratory of Chronobiology, Charité Universitätsmedizin Berlin, Hessische Strasse 3-4, 10115 Berlin, Germany

[5]Present address: Division of Cardiovascular Medicine, Departments of Anesthesia and Medicine, Brigham and Women's Hospital, Harvard Medical School, 75 Francis Street, Boston, MA 02115, USA

[6]Present address: Medical Research Council Laboratory of Molecular Biology, Hills Road, Cambridge CB2 0QH, UK

*Correspondence: eva.wolf@med.uni-muenchen.de

http://dx.doi.org/10.1016/j.cell.2013.05.011

SUMMARY

Drosophila cryptochrome (dCRY) is a FAD-dependent circadian photoreceptor, whereas mammalian cryptochromes (CRY1/2) are integral clock components that repress mCLOCK/mBMAL1-dependent transcription. We report crystal structures of full-length dCRY, a dCRY loop deletion construct, and the photolyase homology region of mouse CRY1 (mCRY1). Our dCRY structures depict Phe534 of the regulatory tail in the same location as the photolesion in DNA-repairing photolyases and reveal that the sulfur loop and tail residue Cys523 plays key roles in the dCRY photoreaction. Our mCRY1 structure visualizes previously characterized mutations, an NLS, and MAPK and AMPK phosphorylation sites. We show that the FAD and antenna chromophore-binding regions, a predicted coiled-coil helix, the C-terminal lid, and charged surfaces are involved in FAD-independent mPER2 and FBXL3 binding and mCLOCK/mBMAL1 transcriptional repression. The structure of a mammalian cryptochrome1 protein may catalyze the development of CRY chemical probes and the design of therapeutic metabolic modulators.

INTRODUCTION

Most organisms exhibit daily cycles of physiology, metabolism, and behavior, so-called circadian rhythms, which are generated by circadian clocks. The roughly 24 hr period results from gene-regulatory negative feedback loops with a spatiotemporally regulated interplay of interactions between and posttranslational modifications, synthesis, and degradation of clock proteins (Young and Kay, 2001).

Drosophila cryptochrome (dCRY) is a flavin adenine dinucleotide (FAD) binding blue-light photoreceptor involved in the synchronization of the circadian rhythm with the environmental light-dark cycle (Emery et al., 1998; Stanewsky et al., 1998) and in light-dependent magnetosensitivity (Gegear et al., 2008).

The mammalian cryptochromes (CRY1, CRY2) act as light-independent integral clock components repressing the mCLOCK/mBMAL1 transcription factor complex in the main feedback loop (Griffin et al., 1999; Kume et al., 1999; van der Horst et al., 1999). The repressor activity is determined by posttranslational modifications, such as CRY phosphorylation by MAPK (Sanada et al., 2004) or mBMAL1 acetylation at Lys537 (Czarna et al., 2011; Hirayama et al., 2007), as well as the daily rhythmic synthesis, degradation, and nuclear translocation of the CRYs, which are controlled by interactions with the E3-ligase FBXL3 (Gatfield and Schibler, 2007) and the mammalian PERIOD (mPER1/2) clock proteins (Yagita et al., 2002). CRY1 also affects glucose homeostasis by interacting with the $G_s\alpha$ subunit of heterotrimeric G proteins and thereby inhibiting cAMP-dependent CREB phosphorylation and activity (Zhang et al., 2010). Additionally, CRY1 and CRY2 interact with the ligand-bound glucocorticoid receptor (GR) and thereby repress the GR-induced expression of the gluconeogenetic enzyme phosphoenolpyruvate carboxykinase 1 (Pck1) in the liver but do not affect glucocorticoid-induced inflammatory genes (Lamia et al., 2011). Compounds that enhance cryptochrome activity or stability could therefore be useful in the treatment of type 2 diabetes or limit hyperglycaemia in anti-inflammatory glucocorticoid treatments. For human CRY2, a blue-light-dependent function as a magnetoreceptor has also been reported when transformed into cry loss-of-function (cry^b, D410N) *Drosophila* flies (Foley et al., 2011). Moreover, human CRY is photoreduced in overexpressing Sf21 insect cells and is degraded in a light-dependent manner in living flies (Hoang et al., 2008).

Cryptochromes and the sequence-related DNA-repairing photolyases share a chromophore binding photolyase homology region (PHR). The PHR consists of an N-terminal $\alpha\beta$ domain and a

C-terminal helical domain, which binds FAD in a U-shaped manner with the isoalloxacine ring adjacent to the adenine (Müller and Carell, 2009). Photolyases also contain antenna chromophores, which funnel energy to the catalytic FAD chromophore. In addition to the PHR, cryptochromes have C-terminal regulatory tail regions of variable length and sequence (Cashmore, 2003).

Purified dCRY binds oxidized FAD in its dark state, which is converted to an anionic $FAD^{\circ-}$ radical after blue-light illumination (Berndt et al., 2007). A cascade of three highly conserved tryptophanes (Trp342, Trp397, and Trp420 in dCRY) has been implicated in the electron transport required for FAD photoreduction (Hoang et al., 2008). The PHR of dCRY interacts with TIMELESS (dTIM) and the E3-ligase JETLAG (JET) in a light-dependent manner, and the tail prevents these interactions in darkness (Busza et al., 2004; Peschel et al., 2009). A light-induced conformational change of the tail allows for dCRY-dTIM/JET interactions (Ozturk et al., 2011) and subsequent JET-dependent proteasomal degradation of dTIM and dCRY (Peschel et al., 2009), which ultimately lead to the light synchronization of the circadian clock.

In mammalian CRYs, the tail and a preceding predicted coiled-coil helix of the PHR mediate interactions with C-terminal mBMAL1 residues (Czarna et al., 2011; Kiyohara et al., 2006; Sato et al., 2006) and thereby repression of mCLOCK/mBMAL1-activated transcription (Chaves et al., 2006). The PHR interacts with C-terminal regions of mPER1 and mPER2 (Miyazaki et al., 2001; Yagita et al., 2002), with the PAS (PER-ARNT-SIM) domains of mCLOCK (Huang et al., 2012) and with FBXL3 (Lamia et al., 2009).

To further elucidate the mechanisms underlying dCRY's photoreceptor function and to dissect the established light-independent and proposed light-dependent functions of mammalian cryptochromes, we have solved crystal structures of full-length dCRY, of a dCRY loop deletion construct, and of the PHR of mouse cryptochrome 1 (mCRY1). Comparison of our dCRY structures with a recently published structure of full-length dCRY (Zoltowski et al., 2011) revealed remarkable differences in the regulatory tail and its adjacent loops, which allowed us to further test and thereby provide insights into the photoactivation mechanism of *Drosophila* cryptochrome. Our mCRY1 structure may guide the design of CRY1 activating or stabilizing compounds that could be used in the therapy of type II diabetes as well as anti-inflammatory glucocorticoid treatments. It also depicts a nuclear localization signal (NLS), MAPK and AMPK phosphorylation sites, and previously analyzed mutations that affect transcriptional repression. Furthermore, our dCRY and mCRY1 structures suggest binding sites for *Drosophila* and mammalian clock proteins. Our mutational analyses revealed partly overlapping mCRY1 regions that are involved in FAD-independent mPER2- and FBXL3 binding and transcriptional repression.

RESULTS AND DISCUSSION

Crystal Structures of *Drosophila* Cryptochrome

We have solved the 2.35 Å crystal structure of a dCRY construct, in which residues Arg294 to Arg298 of the so-called protrusion loop have been deleted (dCRYΔloop). Subsequently, we have solved the 3.2 Å resolution structure of full-length dCRY by molecular replacement using the refined dCRYΔloop structure as a search model (Table S1). Compared to the published dCRY structure (Zoltowski et al., 2011), our dCRY structures show remarkable differences in functionally important regions, such as the regulatory tail and its adjacent loops (Figure 1; Figures S1 and S2 available online). Whereas FAD-contacting residues adopt the same positions in our structures as in the published dCRY structure (Figures S2D and S2E), our electron density does not provide evidence for the reduction of FAD in the crystal because no butterfly bending or change of the angle between the isoalloxazine ring and the ribityl chain is observed (Figures 1B and S2D). Structural differences in the tail helix (α23, Glu528 to Phe535) and the preceding linker (Leu516 to Asn527) lead to a two-amino-acid frameshift between our and the published dCRY structure throughout the tail (Figures 1B and S2C). As a result, the reported phosphorylation site at Thr518 (Zoltowski et al., 2011) is not observed in our structures. Furthermore, our structures depict tail residue Phe534 instead of Trp536 in the position that is occupied by the 6-4 photolesion in DNA-repairing photolyases (Hitomi et al., 2009; Maul et al., 2008) (Figures 1B and S2B–S2F). Phe534 is sandwiched between Trp422 and His478 of the PHR.

The tail is positioned between several loops that are characteristic for the 6-4-photolyase/animal cryptochrome family (Hitomi et al., 2009; Zoltowski et al., 2011): (1) the protrusion loop ($Phe288_{dCRY}$ to Ala306); (2) the phosphate binding loop ($Glu246_{dCRY}$ to Met266), which binds a phosphate ion in the structure of *Arabidopsis thaliana* 6-4 photolyase; (3) the C-terminal lid ($Ser426_{dCRY}$ to Pro440); (4) the loop between α5 and α6 ($Asn150_{dCRY}$ to Tyr158); and (5) the electron-rich sulfur loop, which contains $Met331_{dCRY}$ and $Cys337_{dCRY}$ (Figures 1 and S1).

Compared to the published dCRY structure, we observe drastic changes within the C-terminal lid, which are correlated with the structural rearrangements in the adjacent tail region (Figures 1 and S2B). Furthermore, our wild-type (WT) dCRY structure shows different conformations of the protrusion loop and the phosphate-binding loop (Figure 1A). These changes position *our* Trp536 between Arg298 of the protrusion loop and Pro257 of the phosphate binding loop, which could stabilize the closed, dark-adapted conformation of the tail helix (Figure S2G).

In the dCRYΔloop structure, the truncated protrusion loop and the phosphate binding loop adopt different conformations than in our WT dCRY structure, but $Pro257_{dCRY\Delta loop}$ still packs against Trp536 of the tail (Figure S2G). In the full-length dCRY crystals, the noncrystallographic dimer is stabilized by a disulfide bridge between the two equivalent Cys296 residues in the protrusion loop (Figure S2H). However, we do not observe disulfide linked dCRY homodimers in solution (Berndt et al., 2007), and the strongly reducing cytosolic and nuclear environment disfavors disulfide-bond formation in vivo. Comparison of our WT dCRY and dCRYΔloop structures (Figure S2A) shows that the loop deletion and the resulting absence of the Cys296-Cys296 disulfide bridge in the dCRYΔloop construct do not affect the structure of any other parts of the dCRY molecule. Furthermore, the dCRYΔloop protein shows a WT-like photoreduction activity

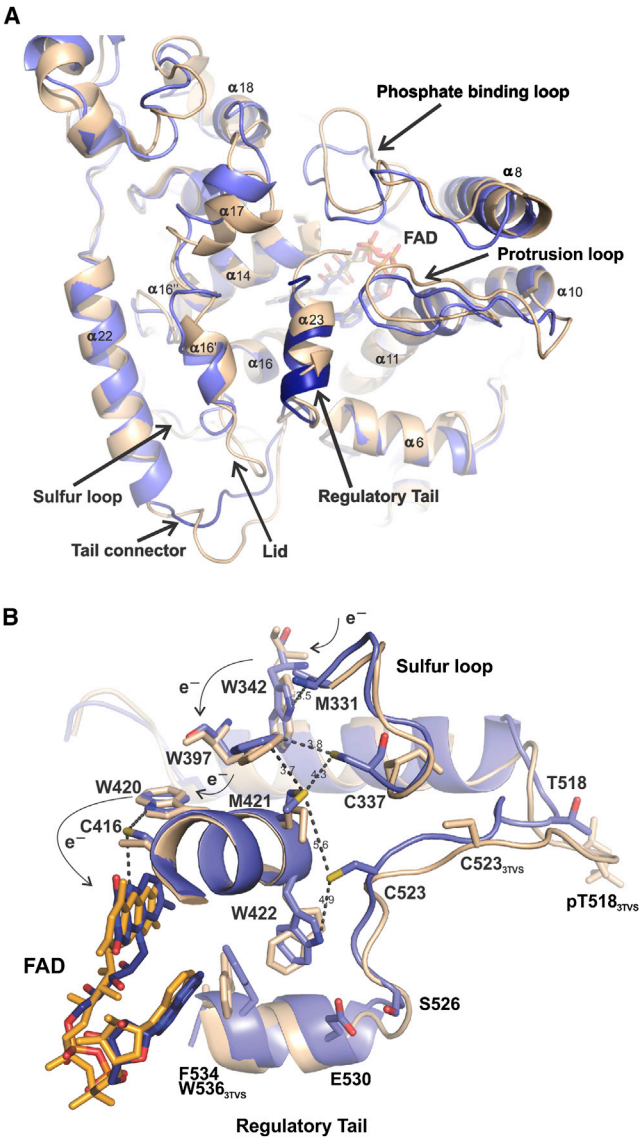

Figure 1. Crystal Structure of Full-Length *Drosophila* Cryptochrome

(A) Superposition of our full-length *Drosophila* Cryptochrome (dCRY) structure (dark blue) with the published dCRY structure (Zoltowski et al., 2011; PDB ID code 3TVS; beige) reveals significant changes in the regulatory tail and adjacent regions, including the protrusion loop, the phosphate binding loop, the C-terminal lid, and the electron-rich sulfur loop.

(B) Our dCRY structure suggests a photoactivation mechanism involving Cys337 and Met331 (sulfur loop) and Cys523 (regulatory tail). Shown as sticks are Trp342, Trp397, and Trp420 (classical Trp cascade), Met331, Cys337, and Cys416 as electron-rich residues gating electron transfer via Trp342, Trp397, and Trp420 (arrows), tail residues Cys523, Ser526, Glu530, and Phe534 (Trp536 in 3TVS), Met421 between Cys523 and Cys337/Trp397, Thr518 (modeled as phospho-Thr518 in 3TVS), Trp422, and FAD. Distances between residues are given in Å. Superposition of our full-length dCRY structure (dark blue) on 3TVS (beige) reveals a two-amino-acid frameshift throughout the tail, displacement of Cys337, and different FAD conformations.

See also Figures S1, S2, and S4 and Table S1.

(Table 1; Figure S3A) and WT-like light-induced conformational changes (Figures S3B and S3C). Hence, the dCRYΔloop structure provides a higher resolution picture of functionally important molecule regions, such as the FAD and antenna chromophore binding regions, the regulatory tail, the C-terminal lid, and the sulfur loop.

Our dCRY structures suggest that Met331 and Cys337 in the electron-rich sulfur loop and Cys523 in the tail connector loop might play a role in the dCRY photoreaction and phototransduction from FAD to the tail (Figure 1B). Reportedly, the mutation of Cys416 (next to Trp420 and the FAD isoalloxazine ring) to alanine accelerates the decay of the anionic $FAD^{\circ-}$ radical, whereas the C416D mutation slows it down (Oztürk et al., 2008). In our dCRY structures, Cys337 is located close to Trp397, the middle tryptophane of the classical electron transfer cascade (Figure 1B). It is conceivable that (due to its electron-rich sulfur atom) Cys337 might slow down the formation and decay of $FAD^{\circ-}$ by gating electron transfer via the $Trp397^{+}$ radical. Moreover, Met331 is in close proximity to Trp342, the outermost classical cascade tryptophane (Figure 1B). We therefore propose that gating of the electron transport at Trp420 (via Cys416), Trp397 (via Cys337), and Trp342 (via Met331) plays a role in determining the lifetime of the light-activated $FAD^{\circ-}$ state and hence the speed and efficiency of dCRY degradation in vivo. The tail residue Cys523 could sense or influence the photoreduction state of FAD via Met421 and Cys337 (Figure 1B).

Our dCRY structures revealed positively and negatively charged dCRY surface regions, which became more extended when the tail was removed (Figure S4). The tail interrupts these charged areas by projecting acidic (Glu528, Glu529) and basic (Arg524, His522) side chains to the surface (Figures S4B and S4C). Because the dTIM protein is acidic (theoretical pI = 5.17) and JET is basic (pI = 8.54), we propose that light-induced displacement of the tail and potential concomitant conformational changes in the tail-adjacent regions could facilitate dTIM or JET binding by removing steric clashes and by generating more extended positively and negatively charged dCRY surface regions.

Functional Analysis of dCRY Reveals Sulfur-Mediated Modulation of the Tryptophan Electron Transfer Cascade

To validate our dCRY structures, we generated dCRY proteins with the single point mutations F534A, E530A/S/R, C523A, S526A (tail), C337A (sulfur loop), and W397F (classical Trp cascade) (Figure 1B). Using UV/VIS spectroscopy, the mutant proteins were analyzed for their effect on the formation and decay of the anionic $FAD^{\circ-}$ radical after blue-light illumination (Table 1). The effect of the mutants on light-induced conformational changes of the tail region was monitored as light-enhanced trypsin cleavage (Ozturk et al., 2011), which gives rise to the formation of two extra cleavage bands (I, II) that are not observed in darkness (Figure 2).

The C337A mutation accelerates the formation and decay of the $FAD^{\circ-}$ radical, whereas the W397F mutation totally abolishes $FAD^{\circ-}$ formation (Table 1). These mutant phenotypes are consistent with our prediction that Cys337 slows down the formation and decay of the $FAD^{\circ-}$ radical by gating electron transport via

Table 1. Photoreduction and Dark Recovery of dCRY

dCRY Protein	Wild-Type	Δloop	W397F or W420F	C416A	C337A	C523A	S526A	E530A/S/R	F534A
Dark recovery time (s)[a]	500 ± 50	500 ± 20	not active	120 ± 10	32 ± 3	82 ± 15	1,125 ± 100	na; proteins insoluble	620 ± 65
Photoreduction time (s)[b]	30	30	not active	30	10	10	30	na; proteins insoluble	30

na, not applicable. See also Figure S3.

[a]Time (t) describing the dark recovery of FAD_{ox} /decay of $FAD^{\circ-}$, which is monitored as an increase of absorbance at 450 nm over time (single exponential fit). Reported values and SDs are the mean of at least three independent experiments.

[b]Time of blue-light illumination (450 nm LED, 5 mW/cm^2 at the sample) required to achieve complete photoreduction of oxidized FAD (FAD_{ox}) to the anionic FAD radical ($FAD^{\circ-}$), measured as the decrease of absorbance at 450 nm.

the adjacent Trp397. In our tryptic digests, the W397F mutation severely inhibits the formation of the light-induced cleavage bands I and II (Figure 2B). The C337A mutant shows WT-like light-induced cleavage kinetics within the first 10 min but seems more active than WT dCRY after 30 and 60 min. Because our dCRY structures do not provide evidence for a direct structural influence of the C337A and W397F mutations on the tail, we propose that the photoreaction kinetics (which are severely affected by these two mutations) play a role in the regulation of tail opening dynamics and hence the lifetime of the signaling state. Interestingly, the C523A mutation also accelerates the formation and decay of the anionic $FAD^{\circ-}$ radical after blue-light illumination (Table 1). We propose that Cys523 might influence the classical tryptophan electron transfer cascade via Met421, which is located nearby Cys523, Cys337, and Trp397 (Figure 1B). The somewhat different kinetics of light-induced trypsin cleavage of the C523A mutant (Figure 2B) likely reflects its altered photoreaction kinetics. A destabilizing effect on the packing of the tail against the PHR (Tyr317-OH, Met321-S, Tyr328-OH, Met421-S, and Trp422-NH; Figure S5A) may also contribute to the overall phenotype of the C523A mutation.

In agreement with published literature (Oztürk et al., 2008), we find that the C416A mutation leads to a WT-like photoreduction speed and faster dark recovery, whereas the W420F mutation totally abolishes formation of the anionic $FAD^{\circ-}$ radical (Table 1). Because the C337A mutation has a more drastic effect on the FAD photoreaction than C416A, we propose that the middle Trp397 of the classical cascade plays a more important role in the regulation of FAD photoreduction and dark recovery kinetics than the innermost Trp420. Further, our dCRY structures and kinetic data suggest that Cys337 communicates with Cys523 in the tail, but there is no obvious communication between Cys416 or Trp420 and the tail (Figure 1B).

Consistent with a structural role of Phe534 stabilizing the interaction of the tail helix with the PHR in the dark-adapted state, the F534A mutation did not significantly affect the formation and decay of the $FAD^{\circ-}$ radical (Table 1) but significantly enhanced the formation of light-induced cleavage bands I and II (Figure 2B). Furthermore, the triple alanine substitution of the Phe534-Phe535-Trp536 motif, which is invariant in type 1 photoreceptor CRYs, reduced dCRY stability in S2 cells under light and dark conditions, whereas the single W536A mutation had little effect (Zoltowski et al., 2011).

Glu530 (tail helix) and Ser526 (tail connector loop) anchor the tail to the PHR by forming hydrogen bonds to each other and to Trp422, Trp314, Tyr158, and Gln159 in the PHR (Figure S5B). Substitutions of Glu530 to Ala, Ser, or Arg resulted in insoluble proteins, which we could not further analyze. Our structure suggests that Ser526 constitutes an essential hinge residue upon opening of the tail (Figure S5B). Consistently, the S526A mutation significantly reduces the light-induced trypsination of dCRY (Figure 2B). In yeast two-hybrid experiments, the mutations S526A and E530P inhibit the light-induced interaction of dCRY with dTIM and dPER, whereas the S526D mutation slightly enhances these interactions (Hemsley et al., 2007). We propose that *Asp526* promotes the open tail conformation by acting in a repulsive manner toward Glu530, whereas *Ala526* and *Pro530* inhibit tail opening by destroying essential hydrogen bonding networks. The S526A mutation also slows down the FAD_{ox} dark recovery by a factor of about two (Table 1), presumably by an indirect mechanism resulting from its effects on the PHR-tail interactions.

Crystal Structure of Mouse Cryptochrome 1

We also report the 2.65 Å crystal structure of the PHR of mouse cryptochrome 1 (mCRY1). Overall, the mCRY1 structure resembles the dCRY and 6-4 photolyase structures but also reveals a number of interesting differences (Figures 3 and 4). The extended loop between helices α6 and α8 ($Met160_{mCRY1}$ to $Gly213_{mCRY1}$) is partly disordered in mCRY1 (missing residues 167 to 177 and 203/204), and the region between $Cys178_{mCRY1}$ and α8 significantly differs from dCRY (Figure 3A). Notably, the phosphorylation of Ser71, which is located in the vicinity of these disordered and structurally variable regions, by 5′AMP-activated protein kinase (AMPK) destabilizes mCRY1, increases its affinity to FBXL3, and weakens mPER2 binding (Lamia et al., 2009). Conceivably, Ser71 phosphorylation restructures or enhances the ordering of its local environment.

Conformational differences are also observed in the protrusion loop, the phosphate binding loop, and the C-terminal lid, which position the tail helix α23 in dCRY (Figures 3A and 3B). The C-terminal lid contains two short α helices (α16', α16'') in dCRY but is unstructured in mCRY1 (Figures 3B and S1). Movement of the C-terminal lid places $Phe405_{mCRY1}$ (corresponding to $Phe428_{dCRY}$) in the location occupied by the tail residue Cys523 in dCRY (Figure 3B; Figures S5C and S5D). The C-terminal lid forms a wall between the FAD binding pocket, the predicted coiled-coil helix α22, and the sulfur loop. Cys412 (lid) forms a disulfide bridge to Cys363 (helix α14), which links the lid to the FAD binding pocket, potentially in a redox-dependent manner (Figure 4C). The loop corresponding to the dCRY protrusion loop is seven residues shorter in mCRY1 and contains an AMPK phosphorylation site at Ser280 (Figures 3A and 3B). The phosphomimetic S280D mutation somewhat reduces mCRY1

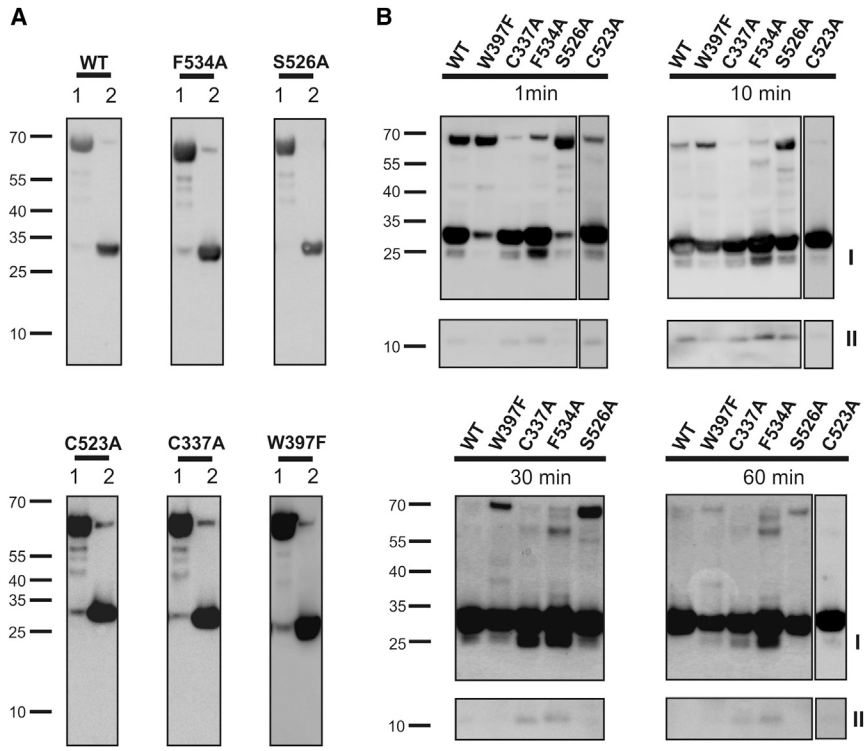

Figure 2. Light Induces Conformational Changes in the dCRY Regulatory Tail

(A) In darkness, trypsin cleaves WT and mutant dCRY proteins at Lys289 in the protrusion loop and generates a roughly 29 kDa band. Lane 1, uncleaved; lane 2, 60 min trypsin cleavage with a 1:20 trypsin:protein (w/w) ratio.

(B) Blue-light illumination of WT and mutant dCRY proteins with a 450 nm LED leads to the formation of two additional trypsin cleavage bands migrating at about 24 kDa (band I) and 11 kDa (band II). Time points: 1', 10', 30', and 60' trypsin cleavage using a 1:20 trypsin:protein (w/w) ratio.

See also Figures S1, S3, and S5.

stability and increases FBXL3 binding but does not affect mPER2 binding (Lamia et al., 2009). The last turn of the α10 helix preceding this loop includes a nuclear localization signal (NLS, K274-K-V-K-K278) (Chaves et al., 2006), and Tyr287/Gly288 in the following helix α11 are critical for transcriptional repression activity (Hitomi et al., 2009; McCarthy et al., 2009). The phosphate binding loop of mCRY1 adopts a different conformation than in dCRY and is partly disordered (Met239 to Asn242 undefined) (Figures 3A and 3B). MAPK phosphorylation of Ser247 (Ser265 in mCRY2) weakens the transcriptional repression activity of mCRY1 and mCRY2 (Hitomi et al., 2009; Sanada et al., 2004), presumably by ordering or restructuring the phosphate binding loop.

Structural Insights into the FAD-Binding Pocket of mCRY1

Our mCRY1 structure was determined in the absence of FAD because our insect-cell-expressed mCRY1 proteins do not bind any chromophores as evidenced by blank absorption spectra. However, comparison of our mCRY1 apo-structure with the FAD-bound dCRY structures reveals only minor changes in the FAD binding pocket (Figures 3C and 3D). Mammalian CRYs might therefore be able to bind FAD after small structural rearrangements, likely dependent on a cellular environment, in which photoreduction and light-dependent magnetoreceptor functions of human CRYs have been reported (Foley et al., 2011; Hoang et al., 2008). Furthermore, the overall positive charge of the empty FAD binding pocket of mCRY1 (Figure 4D) suggests its ability to accommodate FAD or to contribute to electrostatic protein interactions. In all known photolyase and cryptochrome structures, a highly conserved aspartate ($Asp410_{dCRY}$, $Asp387_{mCRY1}$) stabilizes FAD binding by forming a salt bridge to a conserved arginine ($Arg381_{dCRY}$, $Arg358_{mCRY1}$). In our FAD-free mCRY1 structure, Asp387, Ala388, and Arg358 are somewhat moved into the FAD binding site (Figures 3C and 3D). The side chains of His355 and Gln289 are rotated compared to the corresponding $His378_{dCRY}$ and $Gln311_{dCRY}$ and placed in a position that is occupied by FAD in cofactor-bound structures (Figures 3C and 3D; Figure S5D). $His355_{mCRY1}$ also packs against $Arg358_{mCRY1}$ and thereby presumably stabilizes the FAD-free structure. Additionally, the FAD-binding pocket is filled by a number of water molecules (Figure 3C). $Ser265_{dCRY}$ and $Arg237_{dCRY}$, which contact the FAD phosphates in dCRY, are exchanged to Gly250 and His224, respectively, in mCRY1 and moved away from the FAD because they are not used for cofactor binding (Figure 3D).

Implications for mCRY1 Interactions and Transcriptional Repression

Our mCRY1 structure depicts mutations that are reported to influence mPER2 binding or transcriptional repression of mBMAL1/mCLOCK (Figure 4A). Within the predicted coiled-coil helix α22 of mCRY2, Arg501 and Lys503 were shown to be important for mPER2 binding and transcriptional repression activity (Ozber et al., 2010). Moreover, Arg483, Lys485, and Arg478 of mCRY1 are involved in binding of C-terminal mBMAL1 fragments (Czarna et al., 2011). Arg483 (= $Arg501_{mCRY2}$) stabilizes the position of α22 with respect to the PHR by forming stacking interactions with Trp371 and a salt bridge to Asp321 (Figure 4A). Lys485 (= $Lys503_{mCRY2}$) and Arg478 are located on the outer surface of helix α22 and may interact with the negatively charged C-terminal region of mBMAL1 or mPER2 (Figure 4A). Transcriptional repression is also affected by the mutations G106R and R109Q (McCarthy et al., 2009). Gly106 and Arg109 point into the photolyase antenna chromophore binding pocket, which is empty, positively charged and surrounded by a partially disordered loop in our mCRY1 structure (Figures 4A and 4B). Adjacent to the antenna binding pocket, our structure depicts an acidic surface patch that includes Glu375, Glu376, Met378, Glu382 and Glu383 (α15), Asp307, Met309 and Glu310 (sulfur loop),

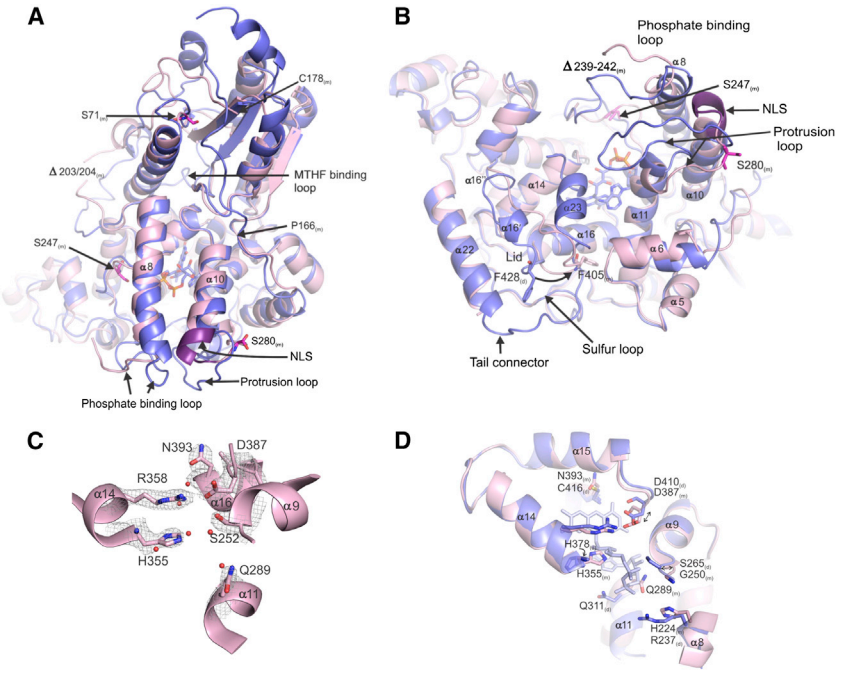

Figure 3. Comparison of mCRY1 and dCRY Crystal Structures

(A) Superposition of mCRY1 (pink) and dCRY (dark blue) structures. AMPK (Ser71, Ser280) and MAPK (Ser247) phosphorylation sites are shown as sticks. The mCRY1-NLS is highlighted in darker pink. (A), (B), and (D): (m), mCRY1; (d), dCRY.

(B) Superposition of mCRY1 with the dCRY tail and adjacent loops reveals structural changes in the protrusion loop, the phosphate binding loop, and the C-terminal lid. Lid movement is manifested by movement of a conserved Phe ($Phe428_{dCRY}$, $Phe405_{mCRY1}$, shown as stick).

(C) FAD binding pocket of mCRY1: residues Ser252, Gln289, His355, Arg358, Asp387, and Asn393 are shown as sticks, and water molecules are as red spheres. The 1.5 sigma 2fo-fc density is shown in gray.

(D) Superposition of mCRY1 and dCRY FAD binding pocket. $Asp387_{mCRY1}$ moves into the FAD binding pocket (black arrow). $His355_{mCRY1}$ and $Gln289_{mCRY1}$ are rotated compared to $His378_{dCRY}$ and $Gln311_{dCRY}$ and would clash with FAD. $Ser265_{dCRY}$ and $Arg237_{dCRY}$ are exchanged to Gly250 and His224 in mCRY1. $Asn393_{mCRY1}$ superimposes with $Cys416_{dCRY}$.

See also Figures S1, S5C, and S5D and Table S1.

Asp321, and Glu332 (Figure 4B). Met309 in the acidic patch, as well as Glu214, Glu216, Ala217, Leu218, and Cys259, are also reported to be involved in transcriptional repression (McCarthy et al., 2009).

Biophysical Analysis of mCRY1-mBMAL1 Interactions

Using isothermal titration calorimetry (ITC), we analyzed the binding of full-length mCRY1 to the C-terminal mBMAL1 fragments mBMAL1[577–625], mBMAL1[490–625], and mBMAL1[490–625]K537Q with an acetyl-lysine-mimetic K537Q mutation. As observed previously for a C-terminal mCRY1 fragment, including helix α22 and the tail (mCRY1CCtail) (Czarna et al., 2011), all binding reactions are endothermic, and the affinity for the mBMAL1[490–625] fragment (K_D = 2 μM) is two times lower than for mBMAL1[577–625] and mBMAL1[490–625]K537Q (K_D = 1 μM) (Figure 5). Hence, the PHR does not appear to affect the ability of the mCRY1 tail to detect $Lys537_{mBMAL1}$ acetylation. The affinities for full-length mCRY1 are, however, ten times higher than for the mCRY1CCtail fragment. Our CD spectra of full-length mCRY1 and a mCRY1Δtail construct imply that the tail has a rather high α-helical content (Table S2; Figure S6). This was not suggested by our CD spectra of the mCRY1CCtail fragment (Czarna et al., 2011). We therefore propose that the PHR restructures the mCRY1 tail region, which likely contributes to the increased mBMAL1 affinity of full-length mCRY1.

Roles of the C-Terminal Lid, the Predicted Coiled-Coil Helix α22, the FAD-Binding Pocket, and Charged Surface Regions for mPER2 and FBXL3 Binding and Transcriptional Repression

To identify mCRY1 regions that regulate mCRY1 stability and transcriptional repression activity, we tested mCRY1 mutants for their effect on mPER2 and FBXL3 binding and transcriptional repression of mCLOCK/BMAL1 using luciferase complementation, fluorescence-two-hybrid, and reporter gene assays in mammalian HEK293 and U2OS cells (Figure 6). The mutations were designed to affect interactions of the C-terminal lid (F405A), the predicted coiled-coil helix α22 (K485D/E, G336D), the FAD binding pocket (H355E, H224E), the phosphate binding loop (S247D), and positively (R437E/K442E/K456E) and negatively (E382R/E383R, E325R) charged mCRY1 surface regions that could play a role in electrostatic protein interactions (Figures 4 and S1).

The C-Terminal Lid Is Involved in mPER2 and FBXL3 Binding, but Not in Transcriptional Repression

The F405A mutation strengthens mCRY1-mPER2 interactions but weakens mCRY1-FBXL3 interactions (Figures 6A and 6B). Our mCRY1 structure suggests that the F405A mutation enhances the flexibility of the C-terminal lid by removing hydrophobic packing interactions of Phe405 to Phe295, Ala299, Met398, Trp399, and Phe306 (Figure S5C). We therefore propose that the F405A mutation stabilizes mCRY1-mPER2 interactions by facilitating necessary conformational changes of the lid. For FBXL3 binding, the integrity of the Phe405 side chain appears to be more important, and therefore, the destabilizing effect of the F405A mutation on the mCRY1-FBXL3 complex becomes predominant. We conclude that the lid interacts with mPER2 and FBXL3, but Phe405 plays different roles in these two interactions. Notably, the F405A mutation does not affect mCRY1's transcriptional repression activity (Figure 6C). Hence, the C-terminal lid does not play a significant role in mCRY1-mCLOCK/mBMAL1 interactions.

Helix α22 Is Involved in mPER2 and FBXL3 Binding as well as Transcriptional Repression

Consistent with earlier reports (McCarthy et al., 2009), the G336D mutant mCRY1 protein shows no repressive activity

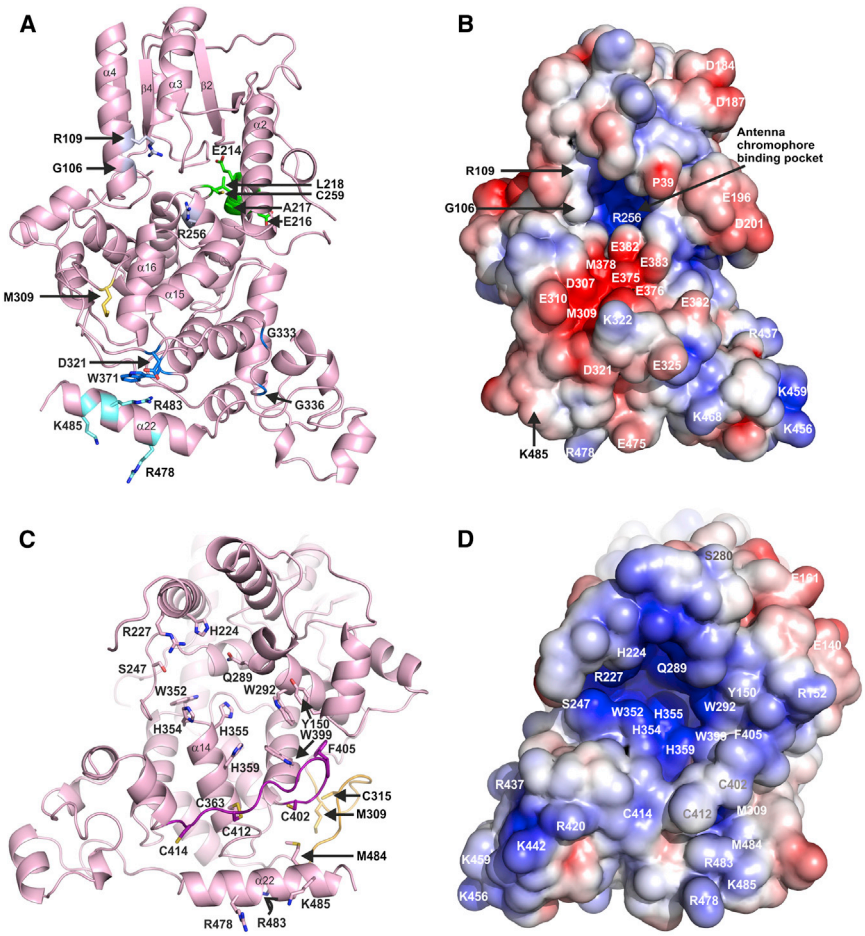

Figure 4. Structural Insight into Functionally Relevant mCRY1 Mutants and Surfaces

(A) Ribbon presentation of mCRY1. Arg478, Arg483, Lys485 (helix α22), Gly336 (near α22 connector loop), Met309 (sulfur loop), Arg109, Gly106 (antenna chromophore binding pocket), Glu214, Glu216, Ala217, Leu218 (α8), and Cys259, which were reported to affect mCRY1 transcriptional repression activity, are shown as sticks. Also depicted are Trp371 and Asp421 (interact with Arg483), Gly333 (G333D mutation affects transcription when tail is deleted), and Arg256 (antenna binding pocket).

(B) Electrostatic surface presentation of mCRY1 highlighting the positively charged antenna chromophore binding pocket (including Arg109, Arg256) and a negatively charged surface patch, including Asp307, Met309, Glu310 (sulfur loop), Glu375, Glu376, Met378, Glu382, Glu383 (α15), Asp321, Glu325, and Glu332. Arg437, Lys456, Lys459, and Lys468 are part of a positively charged surface region that also includes Arg420, Arg437, and Lys422 (see Figure 4D).

(C and D) Close-up view of the FAD binding pocket of mCRY1 (C) and electrostatic surface potential (D). His224, Arg227, Gln289, Trp292, Trp352, His354, His355, His359, and Trp399 form an overall positively charged surface. Cys412 (lid, magenta) forms a disulfide bridge to Cys363 (α14). Cys412 and Cys402 (lid) may form a redox-sensitive platform together with Met309 and Cys315 (sulfur loop, yellow) and Met484 (α22).

(B and D) The colors are ramped from −4 kT/e (red) to +4 kT/e (blue).

See also Figure S1 and Table S1.

toward mCLOCK/mBMAL1 in our assays (Figure 6C). Additionally, the G336D mutation completely disrupts mPER2 binding (Figure 6B). Because Gly336 points toward the loop connecting to helix α22, the G336D mutation is likely to affect mPER2 binding and transcriptional repression by disrupting the orientation of this helix. The K485D/E mutation within helix α22 strongly reduces mPER2 and FBXL3 binding but does not significantly affect transcriptional repression (Figure 6). We therefore propose that mPER2, FBXL3, and mCLOCK/mBMAL1 bind to helix α22 in a somewhat different mode. The strong impact of the K485E/D mutation on mPER2 and FBXL3 binding suggests that both proteins bind to the same side of this helix, which also includes the C-terminal lid as a second common binding element (Figure 6E). The WT-like transcriptional repression activity of the K485D and F405A mutant mCRY1 proteins implies that the mCLOCK/mBMAL1 complex predominantly binds to mCRY1 on the other side of helix α22. Although our peptide substitution analyses suggested that Lys485 is involved in interactions with a C-terminal mBMAL1 fragment (Czarna et al., 2011), this interface may not be essential for stable interactions of the full-length mCRY1 and mCLOCK/mBMAL1 proteins.

The Positively Charged Surface Patch in Helices α17 to α21 Plays a Role in mCRY1-mPER2 Interactions, but Not in Transcriptional Repression and FBXL3 Binding

Helices α17 to α21 preceding the predicted coiled-coil helix α22 include several arginine and lysine residues that together form an extended positively charged surface patch (Figures 4B and 4D). We found that the R437E/K442E/K456E triple mutation significantly enhances mPER2 binding but does not affect transcriptional repression activity and FBXL3 binding (Figure 6). We conclude that Arg437, Lys442, and Lys456 negatively regulate mCRY1-mPER2 interactions without affecting FBXL3 and mCLOCK/mBMAL1.

The Negatively Charged Surface Patch Adjacent to the Antenna Chromophore-Binding Region Plays a Role in mPER2 and FBXL3 Binding as well as Transcriptional Repression

The E382R/E383R double mutation in the negatively charged surface region adjacent to the antenna binding pocket (Figure 4B) leads to an enhanced mPER2 binding, reduced FBXL3 binding, and a significantly reduced transcriptional repression (Figure 6). Hence, Glu382 and Glu383 are required for WT-like FBXL3 binding and transcriptional repression activity of mCRY1 and

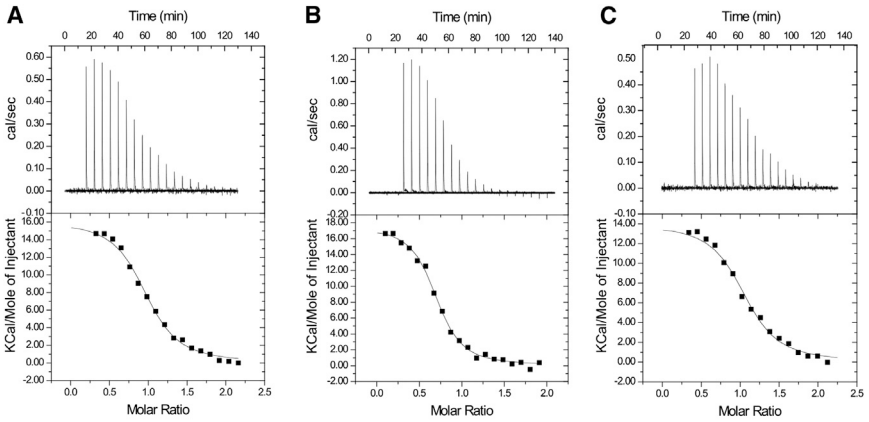

Figure 5. Binding of mBMAL1 to Full-Length mCRY1

(A–C) ITC profiles for interactions of full-length mCRY1 (R, receptor) with mBMAL1 (L, ligand): (A) mBMAL1[577–625] (L: 0.3 mM; R: 0.028 mM), (B) mBMAL1[490–625] (L: 0.55 mM; R: 0.058 mM), and (C) mBMAL1[490–625]K537Q (L: 0.29 mM; R: 0.026 mM). Binding events are endothermic and entropically favored. Top panels: time responses of heat change upon ligand titration. Best fits (lower panels) obtained using a single site binding model with 1:1 stoichiometry (N close to 1).

(D) ITC binding constants and thermodynamic parameters for mCRY1-mBMAL1 interactions. Experiments were done at 22°C. N: number of binding sites (N = ligand/receptor). Reported values and SDs are the mean of at least two independent titrations.

BMAL577 = mBMAL1[577–625]; BMAL490 = mBMAL1[490–625].

See also Figure S6 and Table S2.

D

COMPLEX	N	K_D (μM)	ΔH (kcal/mol)	TΔS (kcal/mol)
mCRY1 / BMAL577	0.9	1.2± 0.2	14.0	20.5
mCRY1 / BMAL490	0.8	2.0± 0.3	18.4	25.7
mCRY1 / BMAL490K537Q	1.0	1.3± 0.2	11.3	19.5

somehow negatively regulate mPER2 interactions. Notably, Gly106 and Arg109 in the antenna binding pocket, as well as Asn393, Asp387 and Arg358 in the FAD binding pocket, which are reported to affect transcriptional repression (Froy et al., 2002; Hitomi et al., 2009; McCarthy et al., 2009), are located nearby Glu382 and Glu383 (Figures 6D and 6E; Figures S7C and S7F). We therefore propose that (1) the acidic surface patch and the antenna recognition region together are involved in transcriptional repression and (2) the D387N/A, N393A/C/D, and R358K/A mutations affect transcriptional repression by disrupting the structural integrity of the acidic surface region rather than FAD binding. Interestingly, the E325R/E382R/E383R triple mutation further enhances mPER2 binding compared to the E382R/E383R double mutation but does not further reduce FBXL3 binding (Figure 6A). The fact that our R437E/K442E/K456E, E382R/E383R, and E325R mutations all enhance mPER2 binding implies that these regions somehow negatively regulate mPER2 binding, possibly by positioning the mCRY1 tail such that it would interfere with mPER2 interactions. Notably, the mutation of Gly333, which is located between Arg437/Lys442/Lys456, Glu382/Glu383, and Glu325 (Figure 6D), to aspartate affects mCRY1 transcriptional repression activity only when the tail is deleted (McCarthy et al., 2009), suggesting the tail to protect Gly333 in the full-length protein.

The FAD-Binding Pocket Is Involved in FBXL3 Interactions

The H355E mutation in the FAD binding pocket leads to a somewhat-enhanced mPER2 binding and a slightly reduced FBXL3 binding in our fluorescence-two-hybrid assay (Figure 6A). Because the H355E mutation would interfere with FAD binding both sterically and by electrostatic repulsion of the phosphate groups (Figures 3C and 3D; Figure S5D), we propose that (1) proper FAD binding is not required for stable mPER2 and FBXL3 interactions and (2) the H355E mutation moderately affects these interactions by modulating the FAD-free structure. The H224E mutation and the phosphomimetic S247D mutation weaken FBXL3 binding but do not significantly change mPER2 interactions (Figure 6A). Moreover, the H224E/H355E double mutation drastically weakens FBXL3 binding but enhances mPER2 binding essentially as the H355E single mutation. We conclude that FBXL3 (but not mPER2) binds across the FAD binding pocket as well as the phosphate binding loop (Figures 4C and 4D). Consistently, a carbazol compound (KL001) that presumably binds to the mCRY1 FAD binding pocket (because its binding is weakened by the D387N and N393D mutations) stabilizes mCRY1 by inhibiting its FBXL3- and ubiquitin-dependent degradation (Hirota et al., 2012).

In summary, several mCRY1-regions are involved in mPER2 interactions, including the C-terminal lid (F405A), helix α14 (H355E), the predicted coiled-coil helix α22 (K485D/E, G336D), and an extended surface area, including positively (R437E/K442E/K456E) and negatively (E382R/E383R, E325R) charged surface regions (Figures 6D and 6E; Figures S7B and S7E). FBXL3 also binds to the lid (F405A), to helix α22 (K485E), and the acidic surface patch (E382R/E383R) but does not interact with the basic helical region (R437E/K442E/K456E) and Glu325. Instead, FBXL3 binds across the FAD binding pocket (H224E/H355E), the phosphate binding loop (S247D), and the protrusion loop (S280D; Lamia et al., 2009) (Figures 6D and 6E; Figures S7A and S7D). Furthermore, the

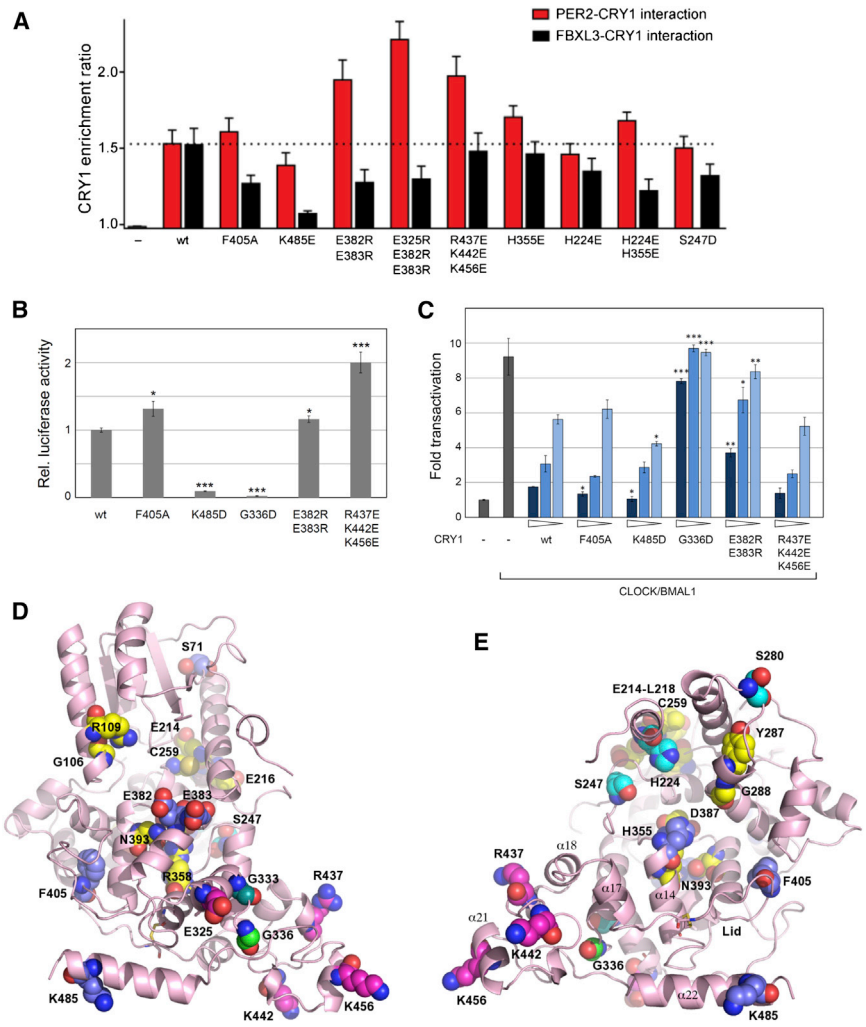

Figure 6. mPER2 and FBXL3 Interactions and Transcriptional Repression Activity of mCRY1 Mutants in Living Cells

(A) Fluorescent two hybrid assays in U2OS cells to assess interactions of WT and mutant mCRY1 with mPER2 (red bar) and FBXL3 (black bar). The enrichment ratio of the prey (mCRY1 WT and mutants) on the Lac-O array spot was quantified by dividing the mean fluorescence intensity on the Lac-O array spot by the mean fluorescence in the nucleoplasm. All values are mean ± SEM, n > 35.

(B) Luciferase complementation assay: full-length mPER2 and mCRY1 (WT or mutants) were expressed as fusion proteins with firefly luciferase fragments in HEK293 cells. The N-terminal luciferase fragment was fused to the C terminus of mPER2 and the C-terminal luciferase fragment to the C terminus of mCRY1. Expression of mCRY1 mutants was verified in western blot experiments (data not shown). Upon binding of mPER2 and mCRY1, a functional luciferase is reconstituted whose activity was measured in cell lysates. Data are normalized to renilla luciferase activity (used as a transfection control) and presented relative to CRY1(WT)-PER2 activity. Shown are mean ± SEM of four independent transfections. (*$p < 0.05$; **$p < 0.005$; ***$p < 0.001$; t test). Two additional experiments gave similar results.

(C) Cotransactivation assay: HEK293 cells were transiently transfected with a firefly luciferase reporter vector containing six E-boxes as well as with plasmids encoding *mClock*, *mBmal1*, and different amounts (100 ng, 20 ng, and 4 ng—symbolized by the triangle) of WT or mutant versions of *mCry1*. Luciferase activity in cell lysates was normalized to renilla luciferase activity (used as a transfection control) and plotted relative to the activity of the reporter only. Shown are mean ± SEM of three independent transfections. (*$p < 0.05$; **$p < 0.005$; ***$p < 0.001$; t test). Two additional experiments gave similar results.

(D and E) mCRY1 ribbon presentation (two orientations as in Figures 4A and 4C) with mutated residues highlighted as colored spheres. Blue: Ser71, His355, Glu382, Glu383, Phe405, and Lys485 affect binding of FBXL3 and mPER2; cyan: His224, Ser247, and Ser280 affect binding of FBXL3, but not mPER2; magenta: Glu325, Arg437, Lys442, and Lys456 affect binding of mPER2, but not FBXL3; light green: Gly336 affects mPER2 binding and transcription; dark green: Gly333 affects transcription when the tail is deleted; and yellow: Gly106, Arg109, Glu214, Glu216, Ala217, Leu218, Cys259, Tyr287, Gly288, Arg358, Asp387, and Asn393 affect mCRY1 transcriptional repression.

See also Figures S1 and S7.

opposing effects of Ser71 phosphorylation on mPER2 and FBXL3 binding (Lamia et al., 2009) suggest that both molecules somehow interact with the N-terminal αβ domain of mCRY1. mPER2 and FBXL3 therefore bind to very extended and partly overlapping mCRY1 surface regions. Whereas the F405A mutation in the lid, the K485D mutation in helix α22, and the R437E/K442E/K456E mutation did not significantly affect transcriptional repression activity, the G336D mutation affecting the positioning of α22 and the E382R/E383R mutation did (Figures 6D and 6E; Figures S7C and S7F). Hence, we have identified helix α22 and the acidic region around Glu382 and Glu383 as two node points that are involved in transcriptional repression as well as mPER2 and FBXL3 interactions and therefore in the regulation of both mCLOCK/mBMAL1 transcriptional activity and mCRY1 stability.

Conclusions

Compared to a recently published dCRY structure (Zoltowski et al., 2011), our dCRY crystal structures reveal a positioning of the regulatory tail and its adjacent loops that offers us substantial mechanistic insights into dCRY function. In particular, our structures and structure-based mutant analyses suggest a mechanism for the light-induced FAD photoreduction that involves gating of the electron transfer via the canonical tryptophan cascade by two cysteines located next to Trp420 (Cys416) and Trp397 (Cys337) and a methionine (Met331) located next to Trp342. Furthermore, our dCRY structures identify (1) Cys523 as a critical tail residue for FAD photoreduction, (2) Phe534 as a central residue that anchors the tail to the PHR and assumes the same location as the photolesion in DNA-repairing photolyases, and (3) Glu530 and Ser526, which anchor the tail to the

PHR via extensive hydrogen bonding networks and are essential for light-induced dCRY-dTIM and dCRY-dPER interactions (Hemsley et al., 2007). Additionally, our structures predict that dTIM and JET bind to basic (dTIM) or acidic (JET) dCRY regions including the tail-adjacent loops.

Our mCRY1 structure depicts AMPK phosphorylation sites at Ser71 and Ser280 that regulate mCRY1 stability in response to the cell's metabolic state (Lamia et al., 2009), a MAPK phosphorylation site at Ser247 (Sanada et al., 2004), and mutations that influence mCRY transcriptional repression activity in the circadian clock (Froy et al., 2002; Hitomi et al., 2009; McCarthy et al., 2009). Our structure-based mutational analyses show that the predicted coiled-coil helix α22, the FAD and antenna chromophore binding regions, the C-terminal lid, the phosphate binding loop, the protrusion loop, and positively and negatively charged surface regions are involved in FAD-independent and partly overlapping mPER2 and FBXL3 interactions and transcriptional repression activities of mCRY1. By revealing distinct features in the FAD and antenna chromophore binding pockets and suggesting mutations that could be tested in vivo for their effects on photoreduction or light-dependent magnetoreceptor functions (Foley et al., 2011; Hoang et al., 2008), our mCRY1 structure will advance the search for potential light- and chromophore-dependent mammalian CRY functions. Furthermore, the structure will inspire the analyses of loop and surface regions that might play a role in mCRY1 interactions with the glucocorticoid receptor (Lamia et al., 2011) or the $G_S\alpha$ subunit of heterotrimeric G proteins (Zhang et al., 2010). Moreover, it will guide the design and optimization of compounds that enhance cryptochrome activity or stability and may be useful in the treatment of type 2 diabetes or limit hyperglycaemia in anti-inflammatory glucocorticoid treatments (Hirota et al., 2012; Lamia et al., 2011; Zhang et al., 2010).

EXPERIMENTAL PROCEDURES

Purification and Crystallization

dCRY and mCRY1 proteins were recombinantly expressed as His-fusions in insect cells. Proteins were purified via Ni-NTA agarose, heparin, anion exchange, and gel filtration columns. Crystals of full-length dCRY and a dCRYΔ[R294–R298] (dCRYΔloop) construct were grown in darkness. They contain two molecules per asymmetric unit. In the mCRY1 crystal setups, full-length mCRY1 protein was spontaneously proteolysed to a mCRY1 [1–497] fragment corresponding to the photolyase homology region (PHR). The mCRY1 crystals contain one molecule per asymmetric unit.

Data Collection, Structure Determination, and Refinement

A 2.35 Å data set of a dCRYΔloop crystal and a 2.65 Å data set of a mCRY1 crystal were collected at beamline X10SA (SLS). A 3.2 Å data set for full-length dCRY was collected at beamline ID23-1 (ESRF). The dCRYΔloop structure was solved by molecular replacement using the *Drosophila* 6-4 photolyase structure (Protein Data Bank [PDB] ID code 2WB2) as a search model. The refined dCRYΔloop structure was used to determine the structures of full-length dCRY and mCRY1 by molecular replacement. Data collection and refinement statistics are summarized in Table S1.

Circular Dichroism Spectroscopy and Isothermal Titration Calorimetry

Circular dichroism (CD) spectroscopy and isothermal titration calorimetry (ITC) were done essentially as described in Czarna et al. (2011).

Blue-Light Illumination and Dark Recovery

UV/VIS absorption spectra were recorded on a Shimadzu UV 1700 spectrometer. A 450 nm LED emitted 5 mW/cm^2 blue-light on the sample. Full-length dCRY and its mutants were photoreduced by blue-light illumination for 5–30 s. Time traces of dCRY dark recovery (FAD_{ox} formation) were recorded at 450 nm.

Partial Proteolysis

For trypsin cleavage, 12 μl of a 0.1 mg/ml sequencing-grade trypsin solution were added to 40 μl of a 0.6 mg/ml full-length dCRY (WT or mutant) protein solution. Tubes were exposed to 450 nm blue light at 1 mW/cm^2 without (light) or with (dark) aluminum foil covers. Reactions were stopped after 0.5, 1, 2.5, 5, 10, 20, 30, and 60 min at 25°C (time course) and resolved by a 4% to 12% SDS-PAGE. Immunoblotting was performed using an anti-dCRY primary antibody (Alpha Diagnostic) and a HRP-conjugated anti-rabbit secondary antibody (GE Healthcare).

Luciferase Complementation Assay

The luciferase complementation assay was performed essentially as described in Kucera et al. (2012).

Cotransactivation Assay

The capacity of mCRY1 mutants to inhibit CLOCK/BMAL1-mediated transactivation from E-box-containing promoters was tested essentially as described in Vanselow et al. (2006).

Fluorescence Two-Hybrid Assay

mPer2 and FBXL3 (bait) were cloned into pmCherry-lacI vectors. WT and mutant mCry1 (prey) were cloned into a pmEGFP-C1 vector. Fluorescence-two-hybrid assays were performed in a lacO (256×) array-containing human U2OS cell line essentially as described in Zolghadr et al. (2008). Imaging was performed on a Zeiss AxioObserver Z1 confocal spinning disk microscope. To quantify mCRY1-mPER2 and mCRY1-FBXL3 interactions, mCRY1 enrichment at the nuclear spot at which the bait protein (mPER2 or FBXL3) was anchored was measured over the nuclear mCRY1 level. The lacI spot was identified by mCherry fluorescence. The recruitment ratio was quantified by dividing the GFP mean fluorescence intensity at the lacI spot (diameter 0.8–3 μm) by the GFP mean fluorescence intensity of the nuclear area surrounding the lacI spot up to 0.96 μm distance.

A detailed description of the Experimental Procedures (cloning, protein expression and purification, crystallization and X-ray structure determination, biochemical, spectroscopic and cell-based studies) is provided in the Extended Experimental Procedures.

ACCESSION NUMBERS

The Protein Data Bank accession numbers for the mCRY1, dCRY, and dCRY-Δloop structures reported in this paper are 4K0R, 4JZY, and 4K03.

SUPPLEMENTAL INFORMATION

Supplemental Information includes Extended Experimental Procedures, seven figures, and two tables and can be found with this article online at http://dx.doi.org/10.1016/j.cell.2013.05.011.

ACKNOWLEDGMENTS

We thank the beamline staff at the Swiss Light Source (SLS, Villingen, CH) and the European Synchrotron Radiation Facility (ESRF, Grenoble) for excellent assistance and our colleagues at the Max Planck Institute of Biochemistry and the Max Planck Institute of Molecular Physiology for help with data collection. We also thank the staff of the Crystallization Facility and the Microchemistry Core Facility of the Max-Planck-Institute of Biochemistry for technical assistance. We are indebted to Michaela Rode for assistance with insect cell culture, Walter Erhardt for the construction of illumination devices, and Jörg Tittor for introduction to the UV/VIS spectrophotometer. We also thank Katja

Schellenberg for the G336D mutant, Helena Breitkreuz for the mCRY1 expression plasmid, Simone Grau for technical assistance, and Ira Schmalen, Torsten Merbitz-Zahradnik, and Justine Witosch for discussions. This work was supported by grants from the Deutsche Forschungsgemeinschaft (WO695-3/4/5/6 to E.W., DFG-funded CIPSM to A.G.L., and SFB740/D2 to A.K.).

Received: May 23, 2012
Revised: February 14, 2013
Accepted: May 3, 2013
Published: June 6, 2013

REFERENCES

Berndt, A., Kottke, T., Breitkreuz, H., Dvorsky, R., Hennig, S., Alexander, M., and Wolf, E. (2007). A novel photoreaction mechanism for the circadian blue light photoreceptor Drosophila cryptochrome. J. Biol. Chem. *282*, 13011–13021.

Busza, A., Emery-Le, M., Rosbash, M., and Emery, P. (2004). Roles of the two Drosophila CRYPTOCHROME structural domains in circadian photoreception. Science *304*, 1503–1506.

Carpenter, A.E., Jones, T.R., Lamprecht, M.R., Clarke, C., Kang, I.H., Friman, O., Guertin, D.A., Chang, J.H., Lindquist, R.A., Moffat, J., et al. (2006). CellProfiler: image analysis software for identifying and quantifying cell phenotypes. Genome Biol. *7*, R100.

Cashmore, A.R. (2003). Cryptochromes: enabling plants and animals to determine circadian time. Cell *114*, 537–543.

Chaves, I., Yagita, K., Barnhoorn, S., Okamura, H., van der Horst, G.T., and Tamanini, F. (2006). Functional evolution of the photolyase/cryptochrome protein family: importance of the C terminus of mammalian CRY1 for circadian core oscillator performance. Mol. Cell. Biol. *26*, 1743–1753.

Czarna, A., Breitkreuz, H., Mahrenholz, C.C., Arens, J., Strauss, H.M., and Wolf, E. (2011). Quantitative analyses of cryptochrome-mBMAL1 interactions: mechanistic insights into the transcriptional regulation of the mammalian circadian clock. J. Biol. Chem. *286*, 22414–22425.

Emery, P., So, W.V., Kaneko, M., Hall, J.C., and Rosbash, M. (1998). CRY, a Drosophila clock and light-regulated cryptochrome, is a major contributor to circadian rhythm resetting and photosensitivity. Cell *95*, 669–679.

Foley, L.E., Gegear, R.J., and Reppert, S.M. (2011). Human cryptochrome exhibits light-dependent magnetosensitivity. Nat. Commun. *2*, 356.

Froy, O., Chang, D.C., and Reppert, S.M. (2002). Redox potential: differential roles in dCRY and mCRY1 functions. Curr. Biol. *12*, 147–152.

Gatfield, D., and Schibler, U. (2007). Physiology. Proteasomes keep the circadian clock ticking. Science *316*, 1135–1136.

Gegear, R.J., Casselman, A., Waddell, S., and Reppert, S.M. (2008). Cryptochrome mediates light-dependent magnetosensitivity in Drosophila. Nature *454*, 1014–1018.

Glas, A.F., Schneider, S., Maul, M.J., Hennecke, U., and Carell, T. (2009). Crystal structure of the T(6-4)C lesion in complex with a (6-4) DNA photolyase and repair of UV-induced (6-4) and Dewar photolesions. Chemistry *15*, 10387–10396.

Griffin, E.A., Jr., Staknis, D., and Weitz, C.J. (1999). Light-independent role of CRY1 and CRY2 in the mammalian circadian clock. Science *286*, 768–771.

Hemsley, M.J., Mazzotta, G.M., Mason, M., Dissel, S., Toppo, S., Pagano, M.A., Sandrelli, F., Meggio, F., Rosato, E., Costa, R., and Tosatto, S.C. (2007). Linear motifs in the C-terminus of D. melanogaster cryptochrome. Biochem. Biophys. Res. Commun. *355*, 531–537.

Hirayama, J., Sahar, S., Grimaldi, B., Tamaru, T., Takamatsu, K., Nakahata, Y., and Sassone-Corsi, P. (2007). CLOCK-mediated acetylation of BMAL1 controls circadian function. Nature *450*, 1086–1090.

Hirota, T., Lee, J.W., St John, P.C., Sawa, M., Iwaisako, K., Noguchi, T., Pongsawakul, P.Y., Sonntag, T., Welsh, D.K., Brenner, D.A., et al. (2012). Identification of small molecule activators of cryptochrome. Science *337*, 1094–1097.

Hitomi, K., DiTacchio, L., Arvai, A.S., Yamamoto, J., Kim, S.T., Todo, T., Tainer, J.A., Iwai, S., Panda, S., and Getzoff, E.D. (2009). Functional motifs in the (6-4) photolyase crystal structure make a comparative framework for DNA repair photolyases and clock cryptochromes. Proc. Natl. Acad. Sci. USA *106*, 6962–6967.

Hoang, N., Schleicher, E., Kacprzak, S., Bouly, J.P., Picot, M., Wu, W., Berndt, A., Wolf, E., Bittl, R., and Ahmad, M. (2008). Human and Drosophila cryptochromes are light activated by flavin photoreduction in living cells. PLoS Biol. *6*, e160.

Huang, N., Chelliah, Y., Shan, Y., Taylor, C.A., Yoo, S.H., Partch, C., Green, C.B., Zhang, H., and Takahashi, J.S. (2012). Crystal structure of the heterodimeric CLOCK:BMAL1 transcriptional activator complex. Science *337*, 189–194.

Kiyohara, Y.B., Tagao, S., Tamanini, F., Morita, A., Sugisawa, Y., Yasuda, M., Yamanaka, I., Ueda, H.R., van der Horst, G.T., Kondo, T., and Yagita, K. (2006). The BMAL1 C terminus regulates the circadian transcription feedback loop. Proc. Natl. Acad. Sci. USA *103*, 10074–10079.

Kucera, N., Schmalen, I., Hennig, S., Öllinger, R., Strauss, H.M., Grudziecki, A., Wieczorek, C., Kramer, A., and Wolf, E. (2012). Unwinding the differences of the mammalian PERIOD clock proteins from crystal structure to cellular function. Proc. Natl. Acad. Sci. USA *109*, 3311–3316.

Kume, K., Zylka, M.J., Sriram, S., Shearman, L.P., Weaver, D.R., Jin, X., Maywood, E.S., Hastings, M.H., and Reppert, S.M. (1999). mCRY1 and mCRY2 are essential components of the negative limb of the circadian clock feedback loop. Cell *98*, 193–205.

Lamia, K.A., Sachdeva, U.M., DiTacchio, L., Williams, E.C., Alvarez, J.G., Egan, D.F., Vasquez, D.S., Juguilon, H., Panda, S., Shaw, R.J., et al. (2009). AMPK regulates the circadian clock by cryptochrome phosphorylation and degradation. Science *326*, 437–440.

Lamia, K.A., Papp, S.J., Yu, R.T., Barish, G.D., Uhlenhaut, N.H., Jonker, J.W., Downes, M., and Evans, R.M. (2011). Cryptochromes mediate rhythmic repression of the glucocorticoid receptor. Nature *480*, 552–556.

Maul, M.J., Barends, T.R., Glas, A.F., Cryle, M.J., Domratcheva, T., Schneider, S., Schlichting, I., and Carell, T. (2008). Crystal structure and mechanism of a DNA (6-4) photolyase. Angew. Chem. Int. Ed. Engl. *47*, 10076–10080.

McCarthy, E.V., Baggs, J.E., Geskes, J.M., Hogenesch, J.B., and Green, C.B. (2009). Generation of a novel allelic series of cryptochrome mutants via mutagenesis reveals residues involved in protein-protein interaction and CRY2-specific repression. Mol. Cell. Biol. *29*, 5465–5476.

Miyazaki, K., Mesaki, M., and Ishida, N. (2001). Nuclear entry mechanism of rat PER2 (rPER2): role of rPER2 in nuclear localization of CRY protein. Mol. Cell. Biol. *21*, 6651–6659.

Müller, M., and Carell, T. (2009). Structural biology of DNA photolyases and cryptochromes. Curr. Opin. Struct. Biol. *19*, 277–285.

Ozber, N., Baris, I., Tatlici, G., Gur, I., Kilinc, S., Unal, E.B., and Kavakli, I.H. (2010). Identification of two amino acids in the C-terminal domain of mouse CRY2 essential for PER2 interaction. BMC Mol. Biol. *11*, 69.

Oztürk, N., Song, S.H., Selby, C.P., and Sancar, A. (2008). Animal type 1 cryptochromes. Analysis of the redox state of the flavin cofactor by site-directed mutagenesis. J. Biol. Chem. *283*, 3256–3263.

Ozturk, N., Selby, C.P., Annayev, Y., Zhong, D., and Sancar, A. (2011). Reaction mechanism of Drosophila cryptochrome. Proc. Natl. Acad. Sci. USA *108*, 516–521.

Peschel, N., Chen, K.F., Szabo, G., and Stanewsky, R. (2009). Light-dependent interactions between the Drosophila circadian clock factors cryptochrome, jetlag, and timeless. Curr. Biol. *19*, 241–247.

Sanada, K., Harada, Y., Sakai, M., Todo, T., and Fukada, Y. (2004). Serine phosphorylation of mCRY1 and mCRY2 by mitogen-activated protein kinase. Genes Cells *9*, 697–708.

Sato, T.K., Yamada, R.G., Ukai, H., Baggs, J.E., Miraglia, L.J., Kobayashi, T.J., Welsh, D.K., Kay, S.A., Ueda, H.R., and Hogenesch, J.B. (2006). Feedback repression is required for mammalian circadian clock function. Nat. Genet. *38*, 312–319.

Sreerama, N., and Woody, R.W. (2000). Estimation of protein secondary structure from circular dichroism spectra: comparison of CONTIN, SELCON, and CDSSTR methods with an expanded reference set. Anal. Biochem. *287*, 252–260.

Sreerama, N., and Woody, R.W. (2004). On the analysis of membrane protein circular dichroism spectra. Protein Sci. *13*, 100–112.

Stanewsky, R., Kaneko, M., Emery, P., Beretta, B., Wager-Smith, K., Kay, S.A., Rosbash, M., and Hall, J.C. (1998). The cryb mutation identifies cryptochrome as a circadian photoreceptor in Drosophila. Cell *95*, 681–692.

van der Horst, G.T., Muijtjens, M., Kobayashi, K., Takano, R., Kanno, S., Takao, M., de Wit, J., Verkerk, A., Eker, A.P., van Leenen, D., et al. (1999). Mammalian Cry1 and Cry2 are essential for maintenance of circadian rhythms. Nature *398*, 627–630.

Vanselow, K., Vanselow, J.T., Westermark, P.O., Reischl, S., Maier, B., Korte, T., Herrmann, A., Herzel, H., Schlosser, A., and Kramer, A. (2006). Differential effects of PER2 phosphorylation: molecular basis for the human familial advanced sleep phase syndrome (FASPS). Genes Dev. *20*, 2660–2672.

Yagita, K., Tamanini, F., Yasuda, M., Hoeijmakers, J.H., van der Horst, G.T., and Okamura, H. (2002). Nucleocytoplasmic shuttling and mCRY-dependent inhibition of ubiquitylation of the mPER2 clock protein. EMBO J. *21*, 1301–1314.

Young, M.W., and Kay, S.A. (2001). Time zones: a comparative genetics of circadian clocks. Nat. Rev. Genet. *2*, 702–715.

Zhang, E.E., Liu, Y., Dentin, R., Pongsawakul, P.Y., Liu, A.C., Hirota, T., Nusinow, D.A., Sun, X., Landais, S., Kodama, Y., et al. (2010). Cryptochrome mediates circadian regulation of cAMP signaling and hepatic gluconeogenesis. Nat. Med. *16*, 1152–1156.

Zolghadr, K., Mortusewicz, O., Rothbauer, U., Kleinhans, R., Goehler, H., Wanker, E.E., Cardoso, M.C., and Leonhardt, H. (2008). A fluorescent two-hybrid assay for direct visualization of protein interactions in living cells. Mol. Cell. Proteomics *7*, 2279–2287.

Zoltowski, B.D., Vaidya, A.T., Top, D., Widom, J., Young, M.W., and Crane, B.R. (2011). Structure of full-length Drosophila cryptochrome. Nature *480*, 396–399.